A New Concept on Remote Sensing of Cirrus Optical Depth and Effective Ice Particle Size Using Strong Water Vapor Absorption Channels Near 1.38 and 1.88 μm

Bo-Cai Gao, Kerry Meyer, and Ping Yang

***Abstract*—Techniques for retrieving cloud optical properties, i.e., the optical depths and particle size distributions, using atmospheric "window" channels in the visible and near-infrared spectral regions are well established. For partially transparent thin cirrus clouds, these "window" channels receive solar radiances scattered by the surface and lower level water clouds. Accurate retrieval of optical properties of thin cirrus clouds requires proper modeling of the effects from the surface and the lower level water clouds. In this paper, we describe a new concept using two strong water vapor absorption channels near 1.38 and 1.88 μm, together with one window channel, for remote sensing of cirrus optical properties. Both the 1.38- and 1.88-μm channels are highly sensitive in detecting the upper level cirrus clouds. Both channels receive little scattered solar radiances from the surface and lower level water clouds because of the strong water vapor absorption below cirrus. The 1.88-μm channel is quite sensitive to changes in ice particle size distributions, while the 1.38-μm channel is less sensitive. These properties allow for simultaneous retrievals of optical depths and particle size distributions of cirrus clouds with minimal contaminations from the surface and lower level water clouds. Preliminary tests of this new concept are made using hyperspectral imaging data collected with the Airborne Visible Infrared Imaging Spectrometer. The addition of a channel near 1.88 μm to future multichannel meteorological satellite sensors would improve our ability in global remote sensing of cirrus optical properties.**

***Index Terms*—Cirrus clouds, meteorology, Moderate Resolution Imaging Spectrometer (MODIS), remote sensing, water vapor.**

I. Introduction

THIN CIRRUS clouds have historically been difficult to detect by satellite sensors with visible and infrared (IR) atmospheric window channels, particularly over land, due to surface emission and the partial transparency of such clouds. However, in the early 1990s, based on the analysis of hyperspectral imaging data collected by the Airborne Visible Infrared Imaging Spectrometer (AVIRIS) [7], [20], it was found that narrow channels near the centers of the 1.38- and 1.88-μm water vapor absorption bands are very useful for detecting thin cirrus clouds [5]. This is because, in the absence of cirrus clouds, little solar radiance in these two bands that is scattered by the surface and lower level water clouds reaches airborne or satellite sensors due to strong water vapor absorption in the lower atmosphere. However, when the high-altitude cirrus clouds are present, the sensor can detect the solar radiation scattered by these clouds. The observations from AVIRIS data strongly influenced the selection and implementation of a channel centered at 1.375 μm with a width of 30 nm on the Moderate Resolution Imaging Spectroradiometer (MODIS) instrument [8], [17] for cirrus detections [4]. At present, cirrus clouds on the global scale are routinely monitored with two MODIS instruments onboard the National Aeronautics and Space Administration (NASA) Terra and Aqua spacecrafts. Global high cloud reflectances in the 0.4–1.0-μm spectral region have also been operationally derived from the MODIS 0.66- and 1.375-μm channel data with an empirical algorithm developed by Gao *et al.* [6]. These reflectance values are related to the optical depths of cirrus clouds [11].

Cirrus clouds are known to have strong influences on the earth's climate system [10]. Modeling and prediction of climate requires the parameterization of cirrus radiative properties, which in return requires the knowledge of cirrus optical properties, i.e., optical depths and particle size distributions. Both the optical depths and particle size distributions can be retrieved from remotely sensed images of atmospheric window channels in the visible and near-IR spectral regions using the well-established bispectral techniques [12]–[14]. The atmospheric window channels detect not only signals from the upper level cirrus clouds; they also receive solar radiances scattered by lower level water clouds and clear land surfaces. When cirrus clouds are located above water clouds or above reflective land surfaces, the retrieval of optical properties of cirrus clouds requires accurate modeling of the lower level water clouds or surface reflectances. Errors in such modeling can potentially introduce errors in the derived cirrus optical properties. In this paper, we describe a technique using two strong water vapor absorption channels near 1.38 and 1.88 μm together with one window channel for simultaneous retrieval of cirrus optical depths and effective ice particle sizes. This technique largely eliminates contaminations from the surface and low-level water clouds because of the use of the strong water vapor absorption channels. We present preliminary results from applications of the technique to hyperspectral imaging data collected with the AVIRIS instrument.

Manuscript received January 12, 2004; revised June 10, 2004. This work was supported in part by the National Aeronautics and Space Administration (NASA) EOS MODIS project, in part by the U.S. Office of Naval Research, in part by the National Science Foundation under CAREER Award Research Grant ATM-0239605, and in part by NASA under Research Grants NAG-1-02002 and NAG5-11935.

B.-C. Gao is with the Remote Sensing Division, Naval Research Laboratory, Washington, DC 20375 USA (e-mail: gao@nrl.navy.mil).

K. Meyer and P. Yang are with the Department of Atmospheric Sciences, Texas A&M University, College Station, TX 77843 USA.

Digital Object Identifier 10.1109/TGRS.2004.833778

II. Background

A. AVIRIS Instrument

AVIRIS is a hyperspectral imaging instrument designed and built at the Jet Propulsion Laboratory [7], [20]. The imaging data acquired with AVIRIS have been used in a variety of research and applications, including geology, agriculture, forestry, coastal and inland water studies, environment hazards assessment, and urban studies [2], [3]. AVIRIS is now an operational instrument with reliable radiometric and spectral calibrations. It has 224 narrow channels with widths of approximately 10 nm to cover the contiguous solar spectral region between 0.4–2.5 μm. AVIRIS typically acquires images with a pixel size of 20 m from a NASA ER-2 aircraft at an altitude of 20 km. The swath width on the ground is approximately 12 km. AVIRIS can also acquire images from a low-altitude aircraft at spatial resolutions of 1–4 m with reduced swath widths.

B. Cirrus Detections

Previously, it was reported [4] that narrow channels near the centers of the 1.38- and 1.88-μm strong water vapor absorption bands are very effective in detecting thin cirrus clouds based on the analysis of AVIRIS data collected in the late 1980s and early 1990s. The mechanisms for cirrus detection are relatively simple. In the absence of cirrus clouds, these narrow channels receive little solar radiance scattered by the surface and low-level water clouds because of the strong absorption of solar radiation by atmospheric water vapor located above them. When the high-level cirrus clouds are present, these channels receive solar radiances scattered by cirrus clouds that contrast well on the dark background.

During the mid-1990s, a major upgrade to the AVIRIS instrument was made. The SNRs of AVIRIS data improved significantly. Here we would like to use the newer AVIRIS datasets to demonstrate again the capability of cirrus detections with narrow channels near 1.38 and 1.88 μm. Fig. 1(a) shows a true-color AVIRIS image (red: 0.66 μm; green: 0.55 μm; blue: 0.47 μm) acquired over Bowie, MD, near a latitude of approximately 38.97°N and a longitude of approximately 76.74°W on July 7, 1996. Surface features are seen through the partially transparent thin cirrus clouds. Fig. 1(b) and (c) shows the 1.38- and the 1.88-μm images, respectively. Both channels allow for the detection of thin cirrus clouds.

C. Cirrus Reflectance Properties

In order to illustrate the reflectance properties of cirrus clouds, we show in Fig. 2 an "apparent reflectance" spectrum measured over an area covered by cirrus clouds above Monterey Bay, CA, on September 4, 1992. Omitting for convenience the wavelength (λ) and cosine-solar-zenith-angle (μ_0) dependencies, we denote the "apparent reflectance" at the aircraft or satellite as

$$\rho^* = \frac{\pi L}{(\mu_0 E_0)} \tag{1}$$

where L is the radiance measured by the satellite and E_0 the extraterrestrial solar flux. The cirrus spectrum was scaled to 0.7 near 0.5 μm in order to avoid the overlapping of this curve with the other two curves in the plot. The absorption features of the atmospheric oxygen band centered near 0.76 μm, water vapor bands near 0.94, 1.13, 1.38, and 1.88 μm, and a carbon dioxide band near 2.06 μm are seen in this spectrum. These features are the result of absorption by atmospheric gases located above and within cirrus clouds. The solar radiation transmitted through cirrus clouds in the downward path is mostly absorbed by atmospheric gases below cirrus and by liquid water in the ocean. The ice absorption

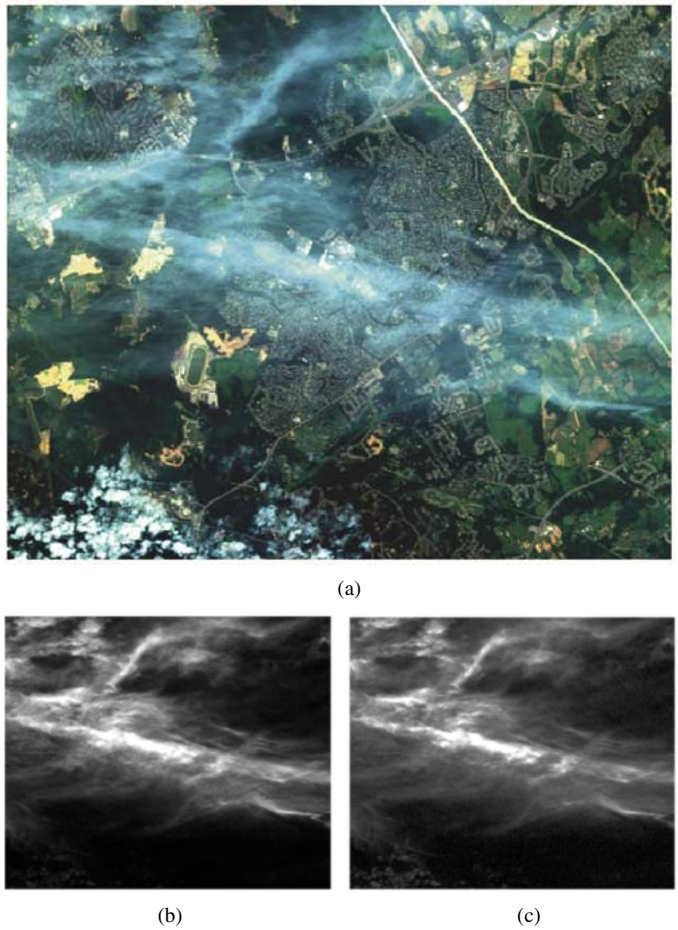

(a) (b) (c)

Fig. 1. (a) True-color AVIRIS image (red: 0.66 μm; green: 0.55 μm; blue: 0.47 μm). (b) The 1.38-μm channel image. (c) The 1.88-μm channel image processed from the AVIRIS data acquired over Bowie, MD, near a latitude of approximately 38.97°N and a longitude of about 76.74°W on July 7, 1996. Surface features are seen in (a), and thin cirrus clouds are seen in (b) and (c).

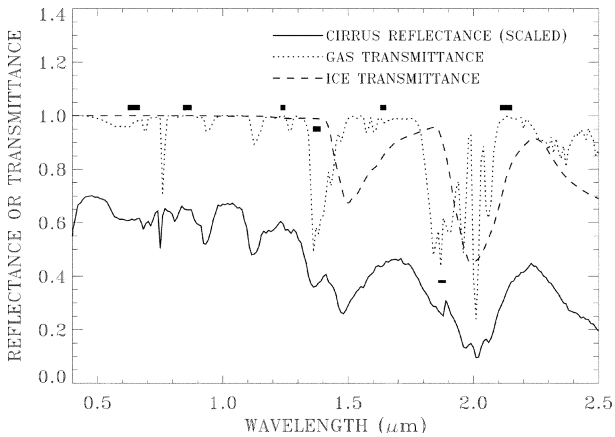

Fig. 2. Cirrus reflectance spectrum measured by AVIRIS over an area above Monterey Bay, Ca, on September 4, 1992, an atmospheric gas transmittance spectrum, and an ice transmittance spectrum.

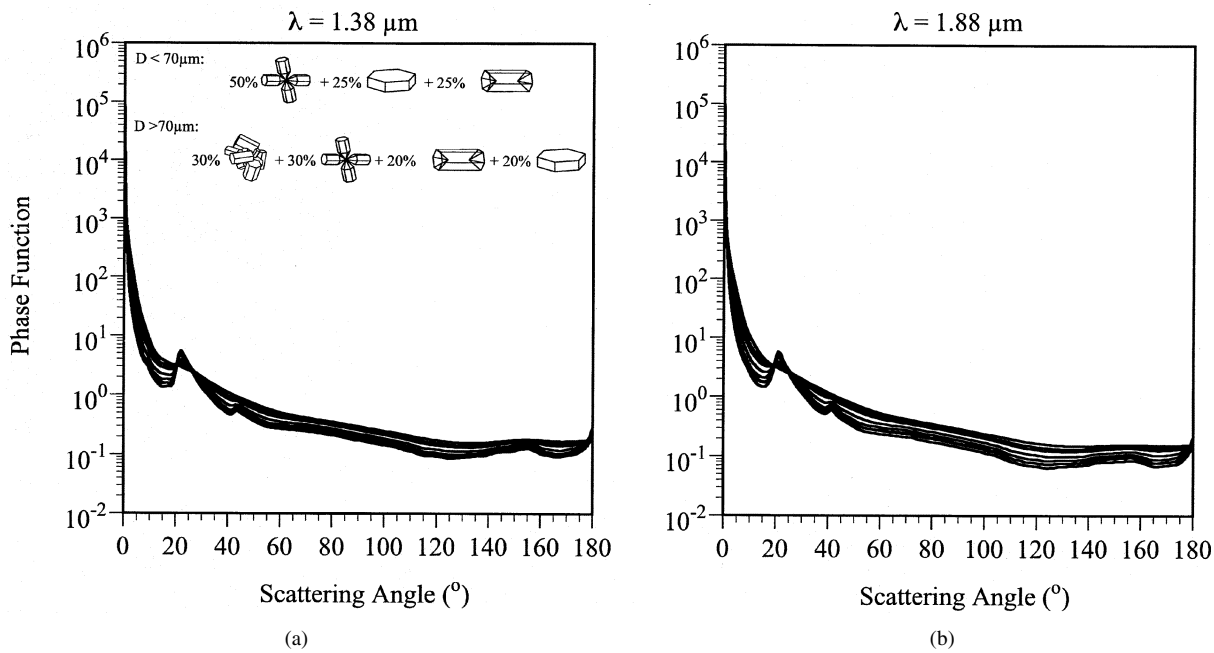

Fig. 3. (a) Scattering phase function plot for the 1.38-μm channel. (b) Scattering phase function plot for the 1.88-μm channel. The habit percentage used in this study is shown in the 1.38-μm plot.

bands centered near 1.5 and 2.0 μm are also seen. These bands result from absorption by ice particles within cirrus clouds. In order to help identify various absorption features contained in the cirrus spectrum, we also show an atmospheric gas transmittance spectrum and an ice transmittance spectrum (0.007 cm thick). Weak ice absorption occurs near 1.24 and 1.38 μm. The effects at both wavelengths are expected to be about the same, since the imaginary parts of the ice refractive index [9] are comparable.

The positions and widths of five MODIS visible and near-IR atmospheric window channels used in the operational retrievals of MODIS cloud optical properties [8], [14] and the 1.375-μm cirrus detecting channel are shown in thick horizontal bars above the transmittance spectra in Fig. 2. A narrow channel centered near 1.88 μm with a width of 30 nm, which is absent in any of the current or near-future meteorological satellite sensors for cirrus detections, is also illustrated with a thinner horizontal bar in the lower right portion of the plot. From the ice transmittance spectrum and cirrus reflectance spectrum, it is seen that the ice absorption effect over the bandpass of the 1.375-μm channel is weak, while the absorption effect over the bandpass of the 1.88-μm channel is stronger. This difference allows, in principle, the simultaneous retrieval of optical depths and ice particle size distributions using both channels with little contamination from the surface or lower level water clouds [see Fig. 1(b) and (c)]. Because the two channels are located within water vapor absorption regions (see the cirrus reflectance spectrum and gas transmittance spectrum), the water vapor absorption effects must be properly modeled and removed before the two channels can be used for the quantitative retrieval of cirrus optical properties.

III. Method

An empirical technique for estimating water vapor transmittances was previously described in detail [5]. Over water surfaces, the scatter plot of the 1.375-μm channel apparent reflectance values ($\rho^*_{1.375}$) versus the 1.24-μm channel apparent reflectance values ($\rho^*_{1.24}$) is made. The slope of an empirically established line is estimated [5], and this slope is considered to be the water vapor transmittance ($T_{1.375}$) for the 1.375-μm channel. Over land surfaces, the water vapor transmittance for the 1.375-μm channel is similarly derived, except that the 0.66-μm channel is used in place of the 1.24-μm channel Because the ice particle absorption effect near 1.375 μm is weak, the intrinsic cirrus reflectance for the 1.375-μm channel, $\rho_{1.375}$, is approximately equal to the ratio of $\rho^*_{1.375}/T_{1.375}$. This intrinsic reflectance is related to the cirrus optical depth [11].

For the 1.88-μm channel, both the atmospheric water vapor absorption effect and the ice particle absorption effect are significant (see Fig. 2). We predict the 1.88-μm channel water vapor transmittance $T_{1.88}$ using the estimated 1.375-μm channel water vapor transmittance $T_{1.375}$ and a line-by-line atmospheric transmittance code [15]. The HITRAN2000 line database [16] is used in the line-by-line calculations. The intrinsic cirrus reflectance for the 1.88-μm channel, $\rho_{1.88}$, is equal to the ratio of $\rho^*_{1.88}/T_{1.88}$. This intrinsic reflectance is related to both the cirrus optical depth and the ice particle size distributions.

After obtaining the intrinsic cirrus reflectances for both the 1.375- and 1.88-μm channels, the retrieval of cirrus optical depth and ice particle size can be made using the well-established Nakajima and King [12] approach. In order to do so, we must first generate lookup tables for each sun/satellite viewing geometry (i.e., relative azimuth angle, as well as solar and viewing zenith angles). Each lookup table should include the 1.38- and 1.88-μm reflectance values, along with the corresponding optical thickness and effective diameter values. The discrete ordinates radiative transfer (DISORT) code [18] is used for all radiance calculations under the assumption of isolated cirrus clouds with no atmosphere above and below the clouds. This assumption is justified because the Rayleigh scattering

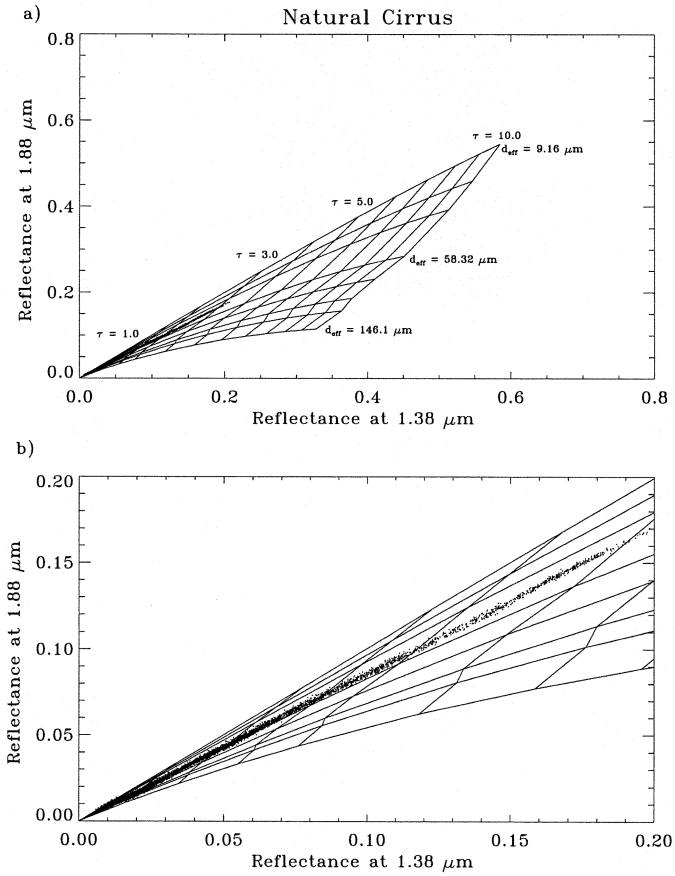

Fig. 4. (a) Sample lookup table for the natural cirrus shown in Scene 3 (236.41° relative azimuth, 44.34° solar zenith, and nadir viewing zenith). (b) Closeup of (a) with Scene 3 AVIRIS data superposed.

effects for wavelengths greater than about 1 μm are negligible. Cirrus scattering properties (used as input for DISORT) are averaged from the results of Yang *et al.* [19].

Fig. 3 shows the single-scattering phase functions for both the 1.38- and 1.88-μm channels averaged from Yang *et al.* [19]. The eight midlatitude size distributions used in the DISORT-generated lookup tables are shown in this plot, with effective diameters ranging from 9.2–46.1 μm. The assumed habit percentages are shown in the 1.38-μm plot. For effective diameters less than 70 μm, we assume a habit percentage of 50% bullet rosettes, 25% plates, and 25% columns. For diameters greater than 70 μm, we assume a composition of 30% rough aggregates, 30% bullet rosettes, 20% columns, and 20% plates [1].

Fig. 4(a) shows a sample lookup table generated for one case study of AVIRIS data (236.41° relative azimuth, 44.34° solar zenith, and nadir viewing zenith). Lines of constant ice crystal effective diameter and cirrus optical thickness are labeled. Note the sensitivity of the 1.38-μm wavelength to optical thickness, and the sensitivity of the 1.88-μm wavelength to effective diameter. For a given pair of intrinsic reflectance values of the 1.38- and 1.88-μm channels, simultaneous retrievals of the optical thickness and ice crystal size distribution can, in principle, be made using the simulated lookup table and a simple table-searching procedure. Fig. 4(b) shows a closeup of Fig. 4(a), with AVIRIS data superposed. The data used in this image are from the natural cirrus image (Scene 3) described below.

IV. Preliminary Results

The method described in Section III has been applied to three sets of AVIRIS data, one containing aircraft-induced contrail cirrus (Scene 1) and two containing natural cirrus (Scenes 2 and 3). Scenes 1 and 2 were taken over the coastal areas of New Jersey on July 12, 1998 during the Long-term Ecosystem Observatory in 15 meter of Water (LEO-15) experiment [21]. LEO-15 was primarily designed for the study of shallow coastal waters. Scene 3 was taken over Monterey Bay, CA, on September 4, 1992. We use the cirrus-contaminated AVIRIS data for our research on simultaneous retrievals of optical depths and ice particle size distributions. The preliminary retrieval results from the three AVIRIS datasets are described below.

A. Contrail Cirrus (Scene 1)

Fig. 5(a) shows the 1.24-μm channel image for the scene containing contrail cirrus. The image covers an area of about 12 km $\times$ 10 km. It has 614 pixels from left to right and 512 pixels from top to bottom. Most of the scene is covered by water, and only a small fraction of the scene is covered by land. The center of the image is located at approximately 39.47°N and 76.25°W. Small white dots are seen throughout the image. These dots represent the wakes of boats in the water. The contrail itself is very thin (very small reflectance), and stretches from left to right across the image. Fig. 5(b) is the 1.38-μm channel image. The contrail cirrus is clearly seen. The boat wakes disappear in this image due to strong absorption by water vapor below the contrail cirrus. Fig. 5(c) shows the 1.88-μm image. It is almost identical to the image in Fig. 5(b) with the exception that the reflectance values are smaller than those of the 1.38-μm channel.

Fig. 6 shows the scatter plot of the 1.38-μm channel apparent reflectance values ($\rho^*_{1.375}$) versus the 1.24-μm channel apparent reflectance values ($\rho^*_{1.24}$) for the scene in Fig. 5. The lower portion of the plot contains land pixels with larger 1.24-μm reflectance values. Pixels covered by the contrail cirrus over the dark water surfaces are clustered around a steep line at left. The slope of this line is our estimate of the water vapor transmittance ($T_{1.375}$) for the 1.375-μm channel. The derivations of the intrinsic cirrus reflectance values for the 1.375-μm channel ($\rho_{1.375}$) and the 1.88-μm channel ($\rho_{1.88}$) are subsequently made using the techniques outlined in Section III. In order to improve the SNRs of the intrinsic cirrus reflectances ($\rho_{1.375}$ and $\rho_{1.88}$), we performed spatial averaging of the data. The resulting dataset has only 76×64 pixels.

During our practical retrieval process, the retrieval code has been written for each set of AVIRIS image data using the computed scene-specific lookup table data. The lookup table resolution is doubled four times (from eight effective diameters and 17 optical depths to 113 effective diameters and 273 optical depths) using linear averaging. We then perform a simple averaging of the optical thickness and effective diameters of the four nearest lookup table points to each data pixel (effectively a data "box").

Fig. 7(a) shows the retrieved cloud optical thickness of the scene in Fig. 5. The plot range is scaled from 0.0–0.4, as displayed on the color bar. The retrieved optical thickness values indicate the very thin nature of this contrail cirrus cloud. The overall pattern of the image clearly matches that of Fig. 5(a)–(c).

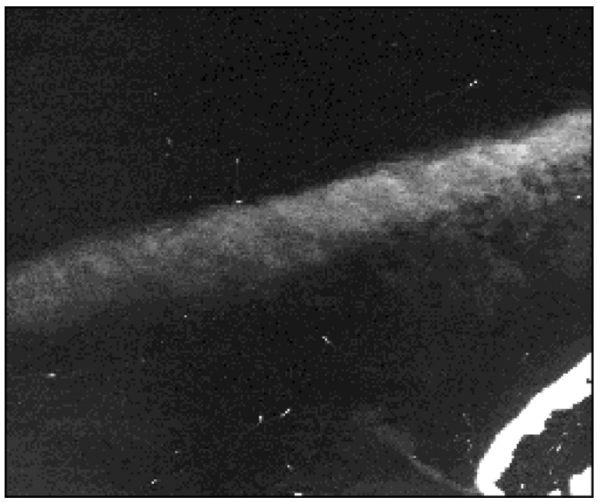

(a)

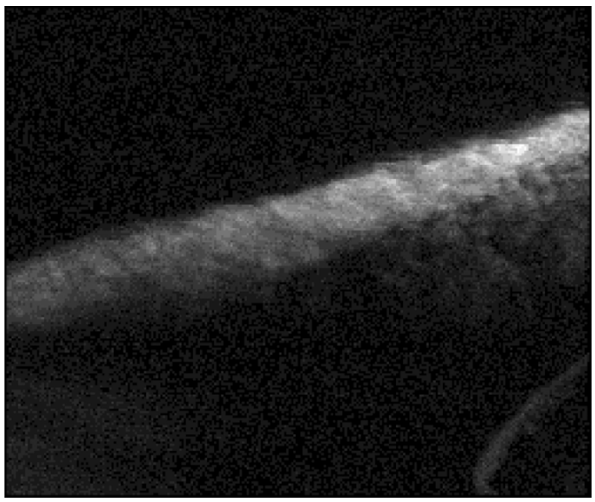

(b)

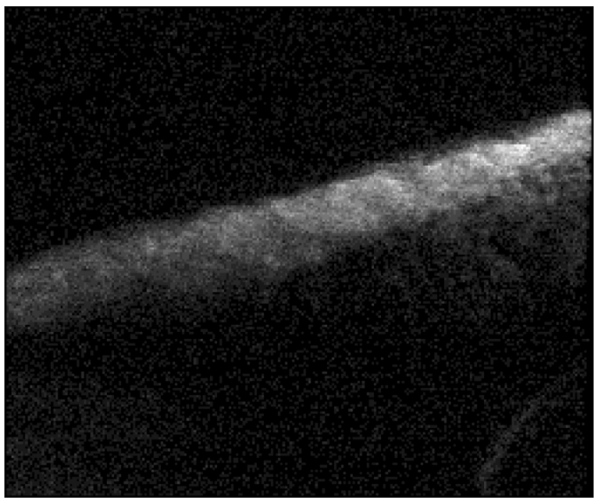

(c)

Fig. 5. (a) AVIRIS 1.24-μm image for Scene 1. (b) AVIRIS 1.38-μm image for Scene 1. (c) AVIRIS 1.88-μm image for Scene 1.

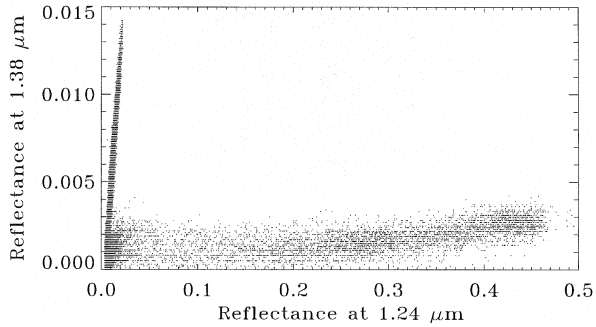

Fig. 6. Scene 1 AVIRIS 1.38- versus 1.24-μm scatter plot. Note the horizontal swath of data points at the bottom of the plot, corresponding to low-level water clouds and surface effects. The steep, narrow swath of points on the left side of the plot indicates cirrus clouds.

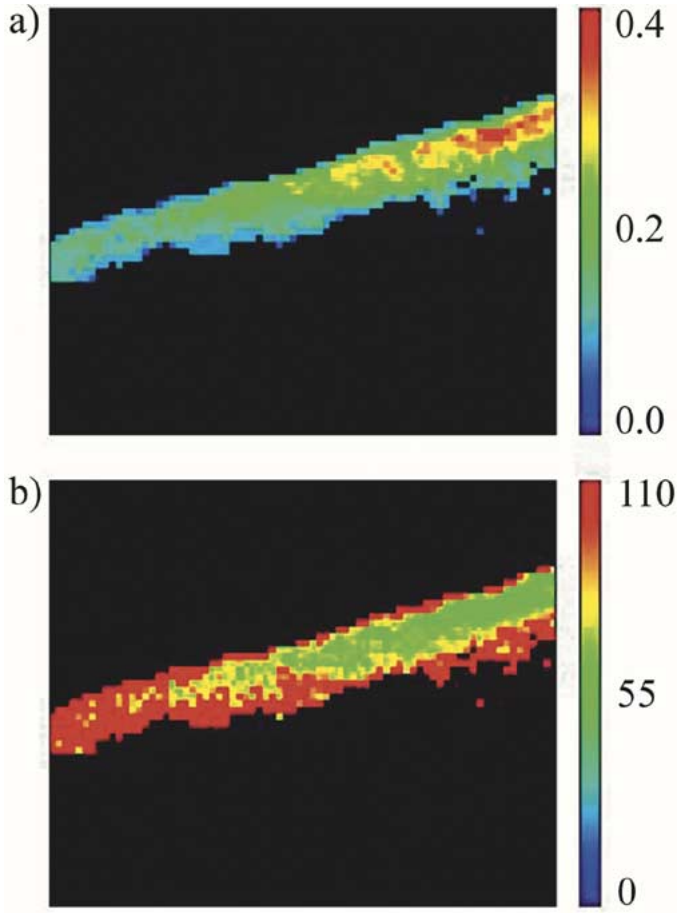

Fig. 7. (a) Retrieved cirrus optical thickness corresponding to the images in Fig. 5 (Scene 1). (b) Retrieved ice crystal effective diameter corresponding to Fig. 5 (Scene 1).

As expected, the largest values of optical thickness are found in the middle portion of the contrail cirrus.

Fig. 7(b) shows the retrieved ice crystal effective diameter of the scene in Fig. 5. The plot range is scaled from 0–110 μm. Again, the overall pattern of the image clearly matches that of Fig. 5(a)–(c). The smallest ice crystal sizes are generally found in the middle of the contrail cirrus (corresponding to large optical thickness values). This is due to a unique aspect of 1.88-μm channel reflectance in that smaller ice crystals reflect more radiation than larger ice crystals, as evidenced by the plot in Fig. 4(b).

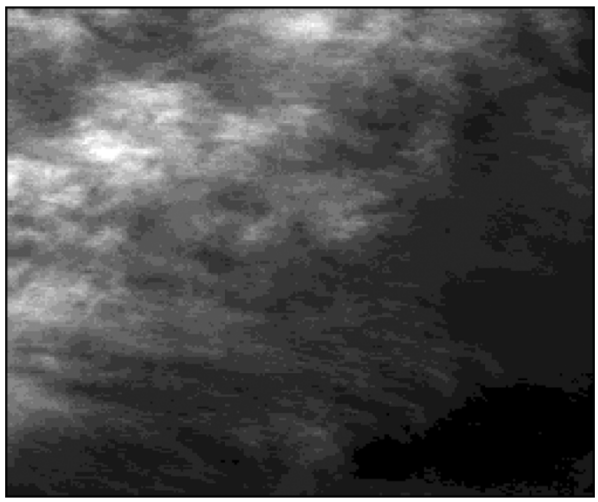

(a)

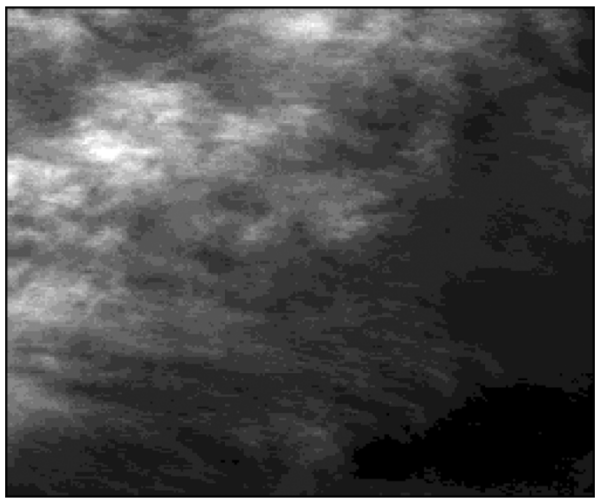

(b)

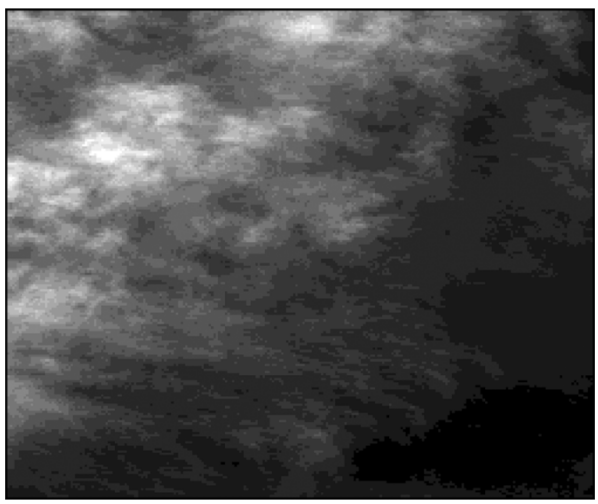

(c)

Fig. 8. (a) AVIRIS 1.24-μm image for Scene 2. (b) AVIRIS 1.38-μm image for Scene 2. (c) AVIRIS 1.88-μm image for Scene 2. Note the similarities between all three images.

B. Natural Cirrus (Scenes 2 and 3)

Fig. 8(a) shows the 1.24-μm channel image for the natural cirrus scene (Scene 2) acquired over the coastal areas of New Jersey. The center of the image is located at approximately 39.47°N and 76.04°W. The entire scene appears to be covered solely by cirrus clouds, with no surface effects. Thick cirrus clouds are evident in the upper left-hand corner of the image. The remainder of the image is covered with relatively thin cirrus. Fig. 8(b) shows the 1.38-μm channel image. This image is very similar to the image in Fig. 8(a). The 1.88-μm channel image is shown in Fig. 8(c). This image also appears very similar to the images in Fig. 8(a) and (b).

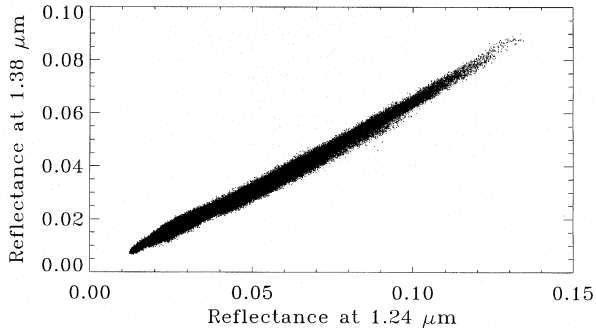

Fig. 9. Scene 2 AVIRIS 1.38- versus 1.24-μm scatter plot. Note that all data points are clustered in a single, narrow swath, indicating the presence of only cirrus clouds.

Fig. 9 shows the scatter plot of the 1.38-μm channel apparent reflectance values ($\rho^*_{1.375}$) versus the 1.24-μm channel apparent reflectance values ($\rho^*_{1.24}$) for AVIRIS Scene 2. Due to the lack of surface and lower level water cloud contributions to the 1.24-μm channel, all the pixels within the scene are very well clustered around a straight line. The slope of this line is our best estimate of the water vapor transmittance ($T_{1.375}$) for the 1.375-μm channel.

Fig. 10(a) shows the retrieved cirrus optical thickness for AVIRIS Scene 2. The plotted range is scaled from 0–2, as displayed on the color bar. The overall pattern of the image clearly matches that of Fig. 8(a)–(c). Maximum values of optical thickness are found in the upper left-hand portion of the plot, corresponding to the areas of high reflectance values in Fig. 8(a)–(c). Smaller optical thickness values are found in the remainder of the image. Unlike the contrail cirrus scene described above, this AVIRIS scene displays a thicker layer of cirrus clouds.

Fig. 10(b) shows the retrieved ice crystal effective diameter for AVIRIS Scene 2. The plotted range is scaled from 0–60 μm, as displayed on the color bar. The overall pattern of this image is much harder to discern than that in Fig. 10(a). However, as should be expected, smaller ice crystals are found in regions of higher cirrus reflectance (and thus larger optical thickness), as evident in the upper left-hand corner of the image. Relatively larger ice crystals comprise the remainder of the image (regions with lower cirrus reflectance). Overall, the retrieved effective diameters in this cirrus image are much smaller than those retrieved for the thin cirrus contrail in Fig. 7(b), as is expected.

Fig. 11(a) shows the 1.24-μm channel image for the second natural cirrus scene (Scene 3) taken over Monterey Bay, Ca. The center of the image is located at approximately 36.83°N and 122.06°W. As in Scene 2, the entire scene appears to be solely covered by cirrus clouds, without apparent surface effects. Major portions of the scene are covered with thin cirrus

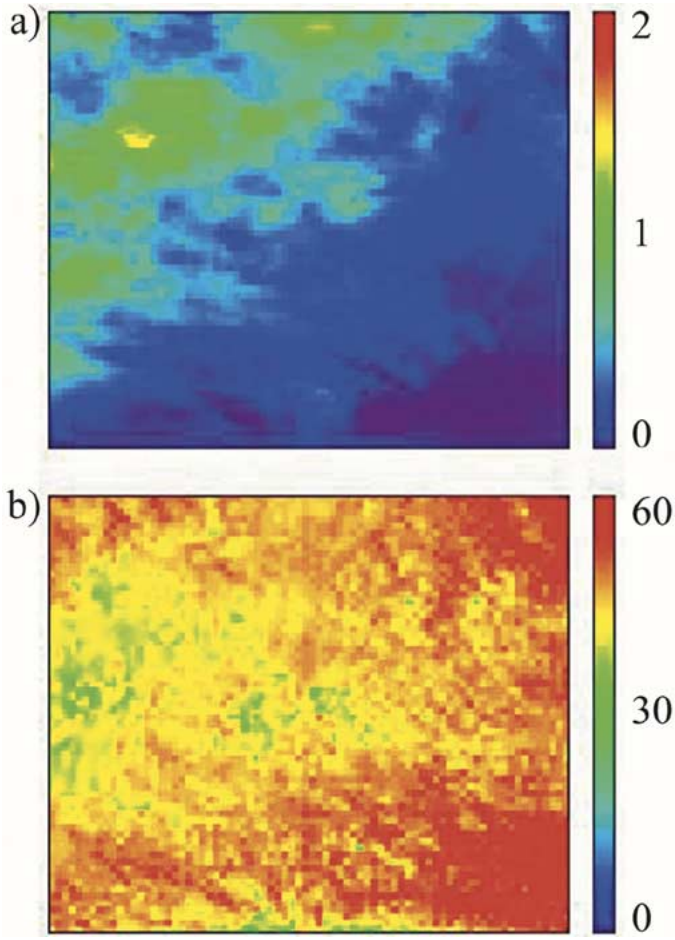

Fig. 10. (a) Retrieved cirrus optical thickness corresponding to the images in Fig. 8 (Scene 2). (b) Retrieved ice crystal effective diameter corresponding to Fig. 8 (Scene 2).

clouds. The upper right portion contains slightly thicker cirrus clouds. The 1.38-μm channel image in Fig. 11(b) is very similar to the Fig. 11(a) image. Fig. 11(c) is the 1.88-μm image corresponding to Fig. 11(a). This image is not as crisp as the images in Fig. 11(a) and (b), due to greater noise in this channel, but still captures the overall pattern of the cloud cover. Thicker cirrus appears in the upper right-hand corner, and thin cirrus is clearly evident throughout the remainder of the scene.

Fig. 12 shows the scatter plot of the 1.375-μm channel apparent reflectance values ($\rho^*_{1.375}$) versus the 1.24-μm channel apparent reflectance values ($\rho^*_{1.24}$) for the scene in Fig. 11. Due to the lack of surface and lower level water cloud contributions to the 1.24-μm channel, all the pixels within the scene are very well clustered around a straight line. The slope of this line is our best estimate of the water vapor transmittance ($T_{1.375}$) for the 1.375-μm channel. The derivations of the intrinsic cirrus reflectance values for the 1.375-μm channel ($\rho_{1.375}$) and the 1.88-μm channel ($\rho_{1.88}$) are then made using the techniques described in Section III. In order to improve the signal to noise ratios of the intrinsic cirrus reflectances, we performed spatial averaging of the data. The resulting dataset has 76×64 pixels. The scatter plot of $\rho_{1.88}$ versus $\rho_{1.375}$ for the spatially averaged data is superposed over the curves generated from the simulated lookup tables, as shown in Fig. 4(b).

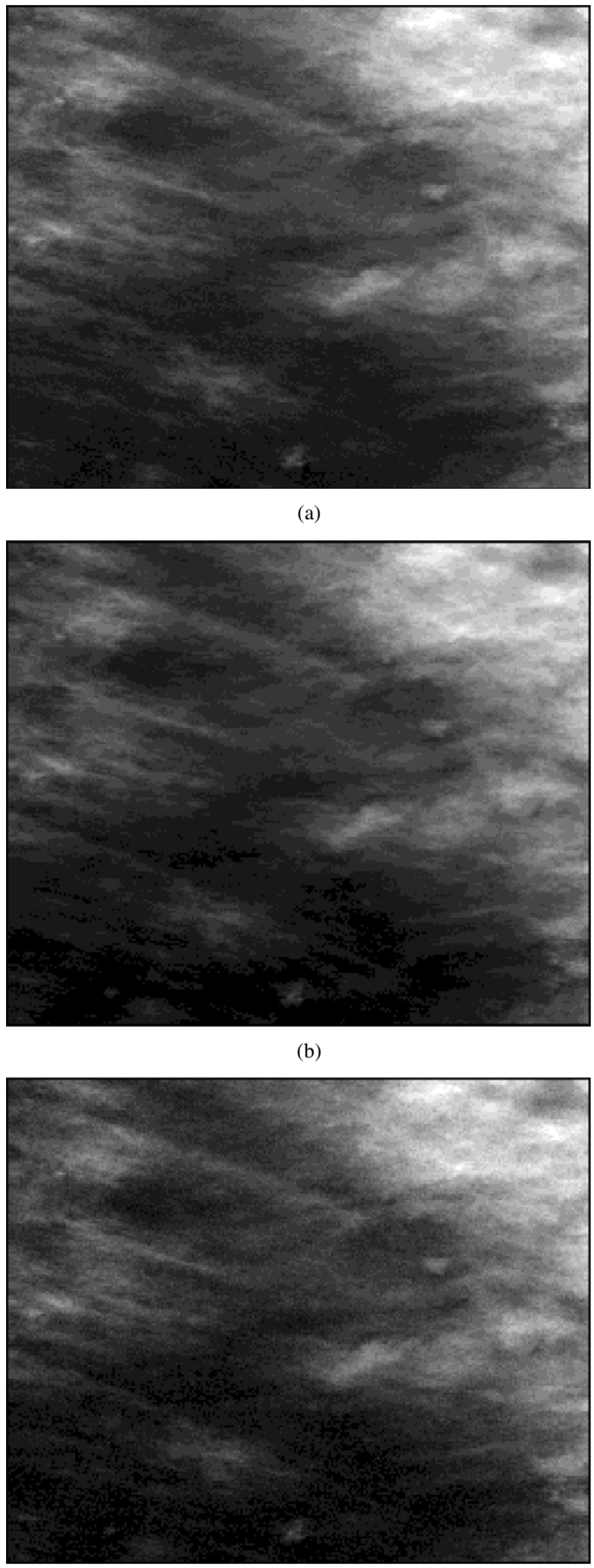

(a)

(b)

(c)

Fig. 11. (a) AVIRIS 1.24-μm image for Scene 3. (b) AVIRIS 1.38-μm image for Scene 3. (c) AVIRIS 1.88-μm image for Scene 3.

The reflectance data in this case was collected before the upgrade to the AVIRIS instrument. We, therefore, apply a lower threshold value of 0.02 on 1.88-μm channel reflectance data. All 1.88-μm channel reflectance values below this threshold, as

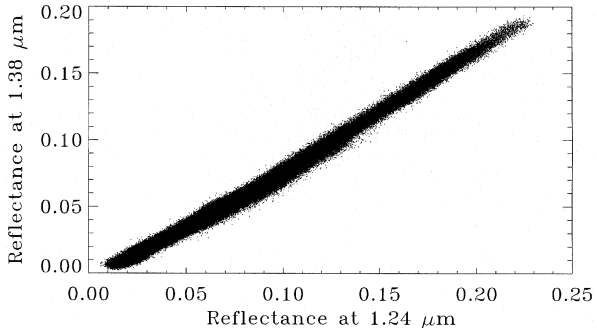

Fig. 12. Scene 3 AVIRIS 1.38- versus 1.24-μm scatter plot. Note that all data points are clustered in a single, narrow swath, indicating the presence of only cirrus clouds.

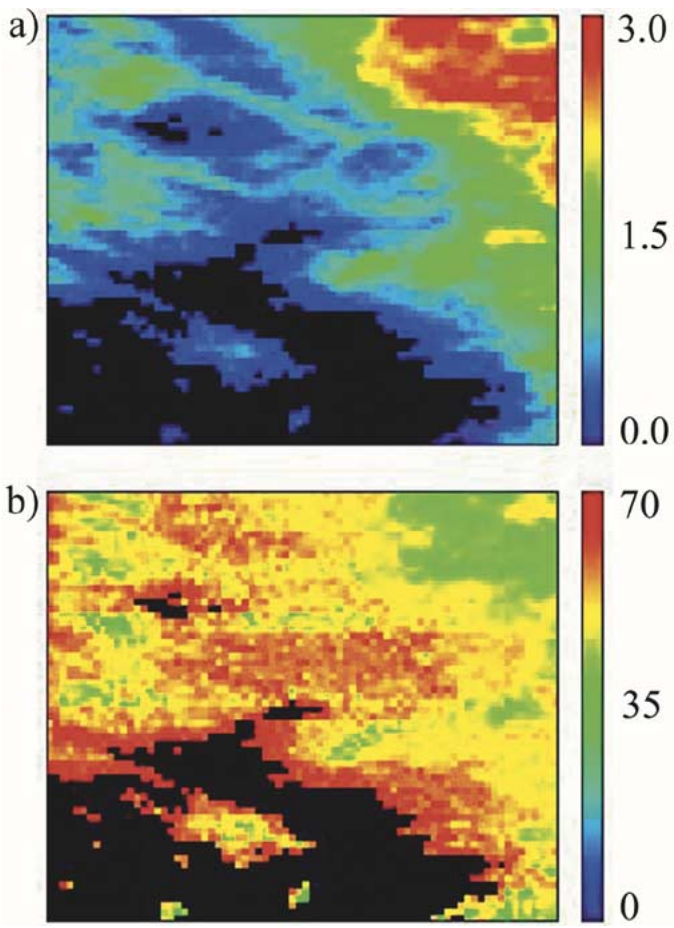

Fig. 13. (a) Retrieved cirrus optical thickness corresponding to images in Fig. 11 (Scene 3). (b) Retrieved ice crystal effective diameter corresponding to Fig. 11 (Scene 3).

well as the corresponding 1.375-μm channel reflectance values, are assumed to be zero (i.e., clear-sky). This is done as a quality-control method to remove noise from the data.

Fig. 13(a) shows the retrieved cloud optical thickness for the scene in Fig. 11. The plotted range is scaled from 0–3, as displayed on the color bar. The overall pattern matches that of Fig. 11(a)–(c). The large, red region of the image corresponds to the region of high reflectance in the upper right-hand corners of Fig. 11(a)–(c). Note that the lower left-hand corner has no retrieved optical thickness. This is a result of the threshold set on the 1.88-μm channel reflectance data to remove noise.

Fig. 13(b) shows the retrieved ice crystal effective diameter of the scene in Fig. 11. The plotted range is scaled from 0–70 μm. Again, the overall pattern matches that of Fig. 11(a)–(c). Note the relatively small retrieved effective diameters in the region of high cirrus reflectance (upper right-hand corner). This is due to the characteristics of the 1.88-μm channel reflectance in that larger reflectance values correspond to smaller ice crystal sizes. Also note the lack of retrieved effective diameter in the lower left-hand corner of the image, again due to the threshold set on the 1.88-μm channel reflectance data.

V. Discussion

Although we marked in Fig. 2 a narrow 1.88-μm channel with a width of 30 nm for remote sensing of cirrus optical properties, the center position and width of the channel should be further refined for implementation of the channel on possible future multichannel meteorological satellite sensors. The atmospheric water vapor absorption and ice particle absorption effects vary rapidly with wavelengths in the 1.7–2.1 μm spectral range. More systematic sensitivity and tradeoff studies are needed in order to optimize the selection of the center position and width of the channel.

A brief analysis of the present method also reveals that potential errors will be relatively small. One major source of error is in our estimation of water vapor transmittance for both the 1.38- and 1.88-μm channels. However, since the transmittance is found using the slope of a linear best fit line from the scatter plots in Figs. 6, 9, and Fig. 12, we expect the error to be on the order of 5% or less. A 1% error in water vapor transmittance corresponds to a slightly greater than 1% error in retrieved cloud optical thickness. Because a water vapor transmittance error translates to errors in both the 1.38- and 1.88-μm channels, the retrieved ice crystal effective size remains virtually unchanged, as evidenced by the lookup table in Fig. 4. Errors in actual reflectance values are insignificant in size and will not affect this study.

VI. Summary

Through analysis of hyperspectral imaging data collected with the AVIRIS instrument, we have established a new concept on simultaneous retrieval of cirrus optical depth and effective ice particle diameter using narrow channels located within the 1.38- and 1.88-μm strong atmospheric water vapor band absorption regions. The theoretically simulated sensitivity curves in Fig. 4 indicate the validity of the new concept. Preliminary tests of the new concept with three sets of AVIRIS data have been made. Quite reasonable optical depths and effective ice particle sizes have been obtained. The implementation of the 1.375-μm channel on MODIS has enabled reliable detection of cirrus clouds on the global scale. It is anticipated that, if an additional narrow channel near 1.88 μm is implemented on a future multichannel meteorological satellite sensor, our ability in global remote sensing of cirrus optical depths and effective ice particle sizes will be improved significantly.

REFERENCES

[1] B. A. Baum, D. P. Kratz, P. Yang, S. C. Ou, Y. Hu, P. F. Soulen, and S. -C. Tsay, "Remote sensing of cloud properties using MODIS airborne simulator imagery during SUCCESS 1. Data and models," *J. Geophy. Res.*, vol. 105, pp. 11 767–11780, 2000.

[2] C. O. Davis, J. Bowles, R. A. Leathers, D. Korwan, T. V. Downes, W. A. Snyder, W. J. Rhea, W. Chen, J. Fisher, W. P. Bissett, and R. A. Reisse, "Ocean PHILLS hyperspectral imager: Design, characterization, and calibration," *Opt. Express*, vol. 10, pp. 210–221, 2002.

[3] B.-C. Gao, K. H. Heidebrecht, and A. F. H. Goetz, "Derivation of scaled surface reflectances from AVIRIS data," *Remote Sens. Env.*, vol. 44, pp. 165–178, 1993.

[4] B.-C. Gao and Y. J. Kaufman, "Selection of the 1.375-μm MODIS channel for remote sensing of cirrus clouds and stratospheric aerosols from space," *J. Atmos. Sci.*, vol. 52, pp. 4231–4237, 1995.

[5] B.-C. Gao, Y. J. Kaufman, W. Han, and W. J. Wiscombe, "Correction of thin cirrus path radiance in the 0.4 – 1.0 μm spectral region using the sensitive 1.375-μm cirrus detecting channel," *J. Geophys. Res.*, vol. 103, pp. 32169–32 176, 1998.

[6] B.-C. Gao, P. Yang, W. Han, R.-R Li, and W. J. Wiscombe, "An algorithm using visible and 1.375-μm channels to retrieve cirrus cloud reflectances from aircraft and satellite data," *IEEE Trans. Geosci. Remote Sensing*, vol. 40, pp. 1659–1688, Aug. 2002.

[7] R. O. Green, M. L. Eastwood, C. M. Sarture, T. G. Chrien, M. Aronsson, B. J. Chippendale, J. A. Faust, B. E. Parvi, C. J. Chovit, M. Solis, M. R. Olah, and O. Williams, "Imaging spectrometry and the Airborne Visible/Infrared Imaging Spectrometer (AVIRIS)," *Remote Sens. Env.*, vol. 65, pp. 227–248, 1998.

[8] M.-D. King, W. P. Menzel, Y. J. Kaufman, D. Tanre, B.-C. Gao, S. Platnick, S. A. Ackerman, L. A. Remer, R. Pincus, and P. A. Hubanks, "Cloud and aerosol properties, precipitable water, and profiles of temperature and humidity from MODIS," *IEEE Trans. Geosci. Remote Sensing*, vol. 41, pp. 442–458, Feb. 2003.

[9] L. Kou, D. Labrie, and P. Chylek, "Refractive indices of water and ice in the 0.65- to 2.5-μm spectral range," *Appl. Opt.*, vol. 32, pp. 3531–3540, 1993.

[10] K. N. Liou, "Influence of cirrus clouds on weather and climate processes: A global perspective," *Mon. Wea. Rev.*, vol. 114, pp. 1167–1198, 1986.

[11] K. Meyer, P. Yang, and B.-C. Gao, "Optical thickness of tropical cirrus clouds derived from the MODIS 0.66- and 1.375-μm channels," *IEEE Transa. Geosci. Remote Sensing*, vol. 42, pp. 833–841, Apr. 2004.

[12] T. Nakajima and M. D. King, "Determination of the optical thickness and effective particle radius of clouds from reflected solar radiation measurements. Part I: Theory," *J. Atmos. Sci.*, vol. 47, pp. 1878–1893, 1990.

[13] S. Platnick, J. Y. Li, M. D. King, H. Gerber, and P. V. Hobbs, "A solar reflectance method for retrieving the optical thickness and droplet size of liquid water clouds over snow and ice surfaces," *J. Geophys. Res.*, vol. 106, pp. 15185–15 199, 2001.

[14] S. Platnick, M. D. King, S. A. Ackerman, W. P. Menzel, B. A. Baum, and R. A. Frey, "The MODIS cloud products: Algorithms and examples from Terra," *IEEE Trans. Geosci. Remote Sensing*, vol. 41, pp. 459–473, Feb. 2003.

[15] W. Ridgway, private communication, 1996.

[16] L. S. Rothman, C. P. Rinsland, A. Goldman, S. T. Messie, D. P. Edwards, J. M. Flaud, A. Perri, C. Camy-Peyret, V. Dana, J. Y. Mandin, J. Schroeder, A. McCann, R. R. Gamach, R. B. Wattson, K. Yoshino, K. V. Chance, K. W. Jucks, L. R. Brown, V. Nemtchinov, and P. Varanasi, "The HITRAN molecular spectroscopic database and HAWKS (HITRAN Atmospheric Workstation): 1996 edition," *J. Quant. Spectrosc. Radiat. Transf.*, vol. 60, pp. 665–710, 1998.

[17] V. V. Salomonson, W. L. Barnes, P. W. Maymon, H. E. Montgomery, and H. Ostrow, "MODIS: Advanced facility instrument for studies of the earth as a system," *IEEE Trans. Geosci. Remote Sensing*, vol. 27, pp. 145–153, Mar. 1989.

[18] K. Stamnes, S.-C. Tsay, W. W. Wiscombe, and K. Jayaweera, "A numerically stable algorithm for discrete-ordinate-method radiative transfer in multiple scattering and emitting layered media," *Appl. Opt.*, vol. 27, pp. 2502–2509, 1998.

[19] P. Yang, K. N. Liou, K. Wyser, and D. Mitchell, "Parameterization of the scattering and absorption properties of individual ice crystals," *J. Geophy. Res.*, vol. 105, pp. 4699–4718, 2000.

[20] G. Vane, R. O. Green, T. G. Chrien, H. T. Enmark, E. G. Hansen, and W. M. Porter, "The Airborne Visible/Infrared Imaging Spectrometer," *Remote Sens. Env.*, vol. 44, pp. 127–143, 1993.

[21] C. J. von Alt, M. P. De Luca, S. M. Glenn, J. F. Grassle, and D. B. Haidvogel, "LEO-15: Monitoring and managing coastal resources," *Sea Technol.*, vol. 38, pp. 10–16, 1997.

Bo-Cai Gao received the B.S. degree from Nankai University, Tianjin, China, in 1982, and the M.S. and Ph.D. degrees from The Ohio State University, Columbus, in 1984 and 1988, respectively, all in physics.

He is currently with the Remote Sensing Division, Naval Research Laboratory, Washington, DC. He has been a member of the MODIS Science Team since 1996, where his focus is on the remote sensing of cirrus clouds, atmospheric water vapor, and coastal water.

Dr. Gao received a Prize Paper Award from the IEEE Geoscience and Remote Sensing Society Symposium (IGARSS) in 1991 for his development of an operational atmospheric radiative transfer code to retrieve surface reflectance spectra from hyperspectral imaging data measured with the NASA/JPL Airborne Visible/Infrared Imaging Spectrometer (AVIRIS).

Kerry Meyer received the B.S. degree in meteorology from Texas A&M University, College Station, in 2001, where he is currently pursuing the M.S. degree in atmospheric sciences.

His research is focused on the remote sensing of cirrus clouds using airborne and satellite data.

Ping Yang received the Ph.D. degree in meteorology from University of Utah, Salt Lake City, in 1995.

He is currently an Assistant Professor in the Department of Atmospheric Sciences, Texas A&M University, College Station. After graduation from the University of Utah, he remained with the university for two years, working as a Postdoctoral Researcher. Later, he was an Assistant Research Scientist at University of California, Los Angeles, as well as with the Goddard Earth Sciences and Technologies Center, University of Maryland Baltimore County, Baltimore, as an Associate Research Scientist. His research interests are in remote sensing and radiative transfer. He has been actively conducting research in modeling of optical and radiative properties of clouds and aerosols, in particular, cirrus clouds and their applications to spaceborne and ground-based remote sensing.